Åström, Jan; Kellomäki, Markku; Alava, Mikko; Timonen, Jussi

Propagation and kinetic roughening of wave fronts in disordered lattices

Published in:
Physical Review E

DOI:
10.1103/PhysRevE.56.6042

Published: 01/11/1997

Document Version
Publisher's PDF, also known as Version of record

Please cite the original version:
Åström, J., Kellomäki, M., Alava, M., & Timonen, J. (1997). Propagation and kinetic roughening of wave fronts in disordered lattices. *Physical Review E*, *56*(5), 6042-6049. https://doi.org/10.1103/PhysRevE.56.6042

Propagation and kinetic roughening of wave fronts in disordered lattices

Jan Åström,[1] Markku Kellomäki,[1] Mikko Alava,[2,3] and Jussi Timonen[1]
[1]*Department of Physics, University of Jyväskylä, P.O. Box 35, FIN-40351 Jyväskylä, Finland*
[2]*NORDITA, Blegdamsvej 17, DK-2100 Copenhagen, Denmark*
[3]*Laboratory of Physics, Helsinki University of Technology, P.O. Box 1100, FIN-02015 HUT, Finland*
(Received 13 June 1997)

The dynamics of a wave front propagating in diluted square lattices of elastic beams is analyzed. We concentrate on the propagation of the first maximum of a semi-infinite wave train. Two different limits are found for the velocity depending on the bending stiffness of the beams. If it vanishes, a one-dimensional chain model is derived for the velocity and the amplitude is found to decrease exponentially. The first maximum is localized and the average width of the wave front is always finite. For very stiff beams an effective-medium model gives the correct velocity and the amplitude of the first maximum decays according to a power law. No localization of the first maximum is observed in the simulations. In this limit scaling arguments based on Huygen's principle suggest a growth exponent of 1/2, and a roughness exponent of 2/3. The growth exponent fits the simulation data well, but a considerably lower roughness exponent (0.5) is obtained. There is a crossover region for the bending stiffness, wherein the wave-front behavior cannot be explained by these limiting cases. [S1063-651X(97)10610-9]

PACS number(s): 46.10.+z, 68.35.Ct, 62.30.+d

I. INTRODUCTION

Propagation of a wave front in a homogeneous and continuous medium is rather well understood within elasticity theory [1]. Wave propagation in a regular lattice is likewise well understood [2]. Almost all real materials, however, contain some kind of disorder such as random microcracks or structural defects. This complicates the situation and interesting phenomena such as localization [3] appear. Disorder also affects the average wave-propagation velocity and the behavior of the wave's amplitude.

We consider here randomly diluted beam lattices as discrete models of elastic solids. As will be demonstrated below, both the amplitude decay and the velocity in randomly diluted lattices can in many cases be found as a function of the dilution parameter. Note that this is made feasible by considering just the first maximum of the wave front, which is much less susceptible to interference. Effects of disorder on amplitude and velocity are, however, just the first characteristics of the wave dynamics. In order to go beyond that, we will investigate in detail also the statistical geometry of the wave fronts in terms of their scaling behavior.

Consider an initially straight wave front. After encountering defects in the medium it will roughen, and the question then is how this happens as measured, e.g., by considering the behavior of the average width of the wave front. The physics behind such changes of shape is best understood by connecting it to the recently much studied concept of kinetic roughening of growing interfaces. Interface growth models usually give rise to self-affine interfaces [4,5], confined to a few universality classes [4] depending on the symmetries of the models. The scaling of self-affine interface growth can be characterized by an initial regime, with a roughness (or wave-front width r) proportional to $r \propto t^{\beta}$, and by an asymptotic regime, characterized by $r \propto L^{\chi}$, where L is the linear system size. In the asymptotic regime the correlation length along the front is of the order of the system size.

One may then ask the question whether wave-front roughening can be characterized by the usual universality classes, despite being governed at long time scales by the Huygens's principle. Consider the simplest growth problems with thermal noise: the random deposition (RD) model [6], the model described by the Edwards-Wilkinson (EW) equation [7], and the model described by the Kardar-Parisi-Zhang (KPZ) [8] equation. The RD universality class describes a set of independent one-dimensional random walks in the direction of wave propagation. This means that roughness grows indefinitely and $\beta = 1/2$. It is quite obvious that no independent one-dimensional paths exist in elastic square lattices, except in special cases such as when the bending stiffness of the bonds vanishes, and therefore the RD model is usually irrelevant in wave-propagation problems.

In the EW and KPZ universality classes there is a surface diffusion term leading to self-affinity and saturation of the roughness in a finite system. The KPZ equation describes kinetic roughening in cases in which local growth always has a finite velocity perpendicular to the interface. As such, one could expect it to be relevant for our problem as indeed is the case for scattered, directed classical waves [9]. We will show below, however, that neither the KPZ nor the EW model is applicable to roughening of wave fronts propagating in a lattice. The only ordinary behavior that can be found belongs, suprisingly enough, to the RD class, which explains the short-time behavior of the wave-front roughness. For the asymptotic behavior, we employ a special argument applicable to interface propagation obeying the Huygens principle.

In the rest of the paper, we begin by describing in detail the lattice model in Sec. II. Section III is devoted to analytical considerations of velocities and amplitude decay of the waves. In Sec. IV we compare analytical results with numerical simulations, and in Sec. V we analyze the roughening of the wave front. Section VI contains conclusions and a discussion.

II. LATTICE MODEL

We study a numerical lattice model because of two reasons: They are efficient from a numerical point of view and represent a straightforward discretization of a brittle solid obeying the Cosserat elasticity equation [10,11]. A discrete lattice can also be considered as a model of a granular material, in which the lattice sites represent the grains and the lattice bonds represent the elastic interactions between the grains. We use a square lattice where the lattice bonds are elastic beams with a square cross section w^2, length l, and Young modulus E. The elastic deformation of a bond is determined by the matrix equation [12]

$$\vec{F} = T^T K_l T \vec{U}, \tag{1}$$

where the vector $\vec{F}$ contains the forces and angular momenta acting on the two ends of the bond, T is a rotation matrix that transforms the local coordinate system of the beam (i.e., the x axis along the beam axis) into the global coordinate system of the lattice, and $\vec{U}$ is the vector containing the displacements related to the forces and momenta in $\vec{F}$. The stiffness matrix K_l in the local coordinate system is given by

$$K_l = \begin{pmatrix} \frac{EA}{l} & 0 & 0 & \frac{-EA}{l} & 0 & 0 \\ 0 & \frac{12EI}{l^3} & \frac{6EI}{l^2} & 0 & \frac{-12EI}{l^3} & \frac{6EI}{l^2} \\ 0 & \frac{6EI}{l^2} & \frac{4EI}{l} & 0 & \frac{-6EI}{l^2} & \frac{2EI}{l} \\ \frac{-EA}{l} & 0 & 0 & \frac{EA}{l} & 0 & 0 \\ 0 & \frac{-12EI}{l^3} & \frac{-6EI}{l^2} & 0 & \frac{12EI}{l^3} & \frac{-6EI}{l^2} \\ 0 & \frac{6EI}{l^2} & \frac{4EI}{l} & 0 & \frac{-6EI}{l^2} & \frac{2EI}{l} \end{pmatrix},$$

where $A = w^2$ and the moment of inertia is $I = w^4/12$. This stiffness matrix holds for small displacements of a slender beam (i.e., shear deformations and nonlinear effects are neglected). The equation governing the elastic response of the entire lattice is easily constructed by summing the stiffness matrices (K_l) for all the bonds in the lattice. Inertia is introduced in the lattice by having masses m on the lattice sites, while the beams are assumed to be massless. Periodic boundary conditions are used in the vertical (y) direction (parallel to one of the principal bond directions). The right boundary is free to move without constraints and the sites at the left boundary are forced to move harmonically [$A_0 \sin(\omega t)$] either in the x or in the y direction when the time $t > 0$. We always use frequencies that are lower than the lowest eigenfrequency of the lattice bonds. The entire lattice is at rest for $t \leqslant 0$.

The dynamics of the lattice is calculated using a discrete form of Newton's equations of motion including a small linear viscous dissipation term,

$$\left[\frac{M}{\Delta t^2} + \frac{C}{2\Delta t}\right] U(t+\Delta t) = \left[\frac{2M}{\Delta t^2} - K\right] U(t) - \left[\frac{M}{\Delta t^2} - \frac{C}{2\Delta t}\right] U(t-\Delta t),$$

where M is the diagonal matrix containing the masses, C is the damping matrix, which is also diagonal, and K is the global stiffness matrix. The time dependent displacement field is calculated by iteration of time steps (Δt) starting from equilibrium at $t = 0$. We follow the first wave front by recording the time when each site in the lattice reaches its first displacement maximum. The location of the front is defined for each lattice row separately so that it is at the site in the row that was the last (before a given time) to reach its first displacement maximum. Disorder is introduced by removing randomly a fraction $1 - p$ of the bonds.

III. VELOCITY AND ATTENUATION OF ELASTIC WAVE FRONTS

A. Anisotropic bond stiffness

First we will derive an approximate solution for the average propagation velocity and the average amplitude decay of the wave front when either the bending or the axial stiffness of the bonds is much smaller than the other. The boundary conditions have been chosen so that the wave front is, in a statistical sense, invariant under transformations in the y direction. Therefore, it is possible to use a one-dimensional model to describe the wave-propagation velocity. The first displacement maximum travels along paths of bonds that are oriented in the x direction. These paths are connected via vertical bonds. Consequently, if the bending stiffness of the bonds is much smaller than their axial stiffness, the vertical bonds will not affect much the velocity of this wave front (i.e., for longitudinal waves induced at the left boundary of the lattice and vice versa for transverse waves). In this case, the velocity can be calculated by approximating the lattice with an ensemble of noninteracting paths of bonds. The equations of motion for such paths are simple one-dimensional wave equations (with zero dissipation)

$$m\frac{d^2u}{dt^2} - kl^2\frac{d^2u}{dx^2} = 0, \tag{2}$$

where $u(x,t)$ are the displacements from equilibrium of the sites, l is the length of a lattice bond, $k = Ew^2/l$ for axial displacements, and $k = (w/l)^2 Ew^2/l$ for transverse displacements. The latter is the bending stiffness of a beam with clamped ends, which can be used if the moment of inertia of the sites is large. To cross the lattice from one side to the other, the wave front will have to travel a distance L_x in the x direction with a local velocity v_x. At each missing horizontal bond, the wave will have to travel at least one unit step in the vertical direction. When p is far above its critical value at percolation, only small connected clusters of missing bonds are present. In this case, the probability that at any lattice site the wave will have to travel at least a step in the vertical direction is approximately $1 - p$. The probability for moving at least two steps vertically is approximately $(1-p)^2$, etc. Thus we approximate the vertical travel dis-

tance by $L_y \simeq L_x \Sigma_{i=1}^{\infty}(1-p)^i$. The local velocity in this direction is v_y. The velocities v_x and v_y are given by $v_x = \sqrt{Ew^2 l/m}$ and $v_y = w/l\sqrt{Ew^2 l/m}$ for induced longitudinal waves (and vice versa for transverse waves). The average wave-front velocity of a longitudinal wave induced at the left boundary of the lattice is then given by

$$v_l(p) = \sqrt{\frac{Ew^2 l/m}{1+(1/p-1)l/w}}, \tag{3}$$

and the corresponding velocity of an induced transverse wave by

$$v_t(p) = w/l\sqrt{\frac{Ew^2 l/m}{1+(1/p-1)w/l}}. \tag{4}$$

B. Effective-medium theory for isotropic bond stiffness

As already mentioned, Eq. (3) [Eq. (4)] is expected to hold when the bending [axial] stiffness is so small that longitudinal [transverse] waves can be considered to propagate along noninteracting paths. This means that the lattice will not reach a local elastic equilibrium during the passage of the first displacement maximum. If, on the other hand, the bending stiffness of the bonds is roughly equal to their axial stiffness, the lattice will locally remain at an elastic equilibrium if the wavelength is not very short. In such a case the lattice will behave as an effectively homogeneous material and the wave-front velocity is determined by the effective Young modulus and the effective Poisson ratio of the lattice.

The effective Young modulus can be calculated within the effective-medium approximation [13]. If one assumes that the elastic deformation of a bond is completely determined by a single constant, the elasticity of a lattice is formally the same as the electric conductance of the lattice with resistors replacing the elastic beams. If the bending stiffness is different from the axial one, it is required that a bond is deformed through either bending or stretching for the formal similarity to hold. In such a case, a fiber that is only bent is considered to have a conductance b, which corresponds to the bending modulus, and a bond that is only stretched has a conductance a, which corresponds to the axial modulus. Notice that this is the so-called Born model [14] of elasticity.

For a square lattice with boundary conditions as described above, it is reasonable to assume that, for induced longitudinal waves, the vertical bonds are only bent and the horizontal bonds are only stretched. The effective-medium approximation is based on the direction symmetry of the current field caused by a point source in an infinite lattice [13]. This symmetry holds only when $a=b$. In the case when $a \neq b$ the situation is somewhat complicated. When p is close to unity the correct solution is obtained by scaling the y direction by a factor $\sqrt{b/a}$. On the other hand, when p is close to the percolation threshold ($p=0.5$ for a square lattice), we expect the direction symmetry to be valid independent of a and b. In our effective-medium solution we use a linear interpolation between these two extremes.

Carrying out the effective-medium calculation as in Ref. [13] gives the effective Young modulus of the lattice in the form

$$E = E_0\{p-[(2-2p)+(2p-1)\sqrt{a/b}](1-p)\}, \tag{5}$$

and the corresponding effective shear modulus in the form

$$\nu = \nu_0\{p-[(2-2p)+(2p-1)\sqrt{b/a}](1-p)\}, \tag{6}$$

where E_0 and ν_0 are the Young modulus and the shear modulus of the perfect lattice. Since the Poisson ratio is zero for a square lattice, the velocity of induced longitudinal waves is given by

$$v_l = \sqrt{\frac{Ew^2 l}{m}\left[p-\left((2-2p)+(2p-1)\frac{l}{w}\right)(1-p)\right]} \tag{7}$$

and the velocity of induced transverse waves by

$$v_t = \frac{w}{l}\sqrt{\frac{Ew^2 l}{m}\left[p-\left((2-2p)+(2p-1)\frac{w}{l}\right)(1-p)\right]}. \tag{8}$$

Both Eqs. (3) and (4) and Eqs. (7) and (8) predict the correct velocities for $p=1$. At the percolation critical point ($p=0.5$) the wave-front velocity is zero (the shortest connected route in a network is fractal at this point). At and close to this point the model of one-dimensional paths fails. The effective-medium model predicts the velocity correctly at the critical point itself (the mean-field critical point is exact for the two-dimensional square lattice), but it fails within the critical region close to the critical point. A better result within this region could, at least in principle, be obtained using the renormalized effective-medium approximation [15].

C. Attenuation

In the case of anisotropic bond stiffness the sawtooth chain model can be applied again for estimating the amplitude decay as a function of p. As long as the wave front travels along an unbroken horizontal chain of bonds, the amplitude remains more or less constant. When the wave front meets a missing bond, it must switch to a neighboring row which takes some time. Meanwhile the wave front propagating along that neighboring row has propagated past the part of the front that switches row. Thus part of the energy of the front propagating in the original row is delayed and we can assume that the amplitude is reduced to a fraction γ of its value at each missing bond (we assume here that one wavelength covers only one or at most a few missing horizontal bonds). With γ being constant the amplitude decays exponentially. The decay as a function of x is then given by

$$A(x) = A_0 \exp[-(1-p)(1-\gamma)x]. \tag{9}$$

There also appears backscattering from missing bonds. In the case of the first maximum of the propagating wave train this effect is negligible, however.

In the case of isotropic bond stiffness the effective-medium approximation is expected to hold. In this approximation, the network is considered as homogeneous, which implies that there will be no amplitude decay at all. However, we must take into account that the network is discrete and therefore dispersion of velocities appears. We have

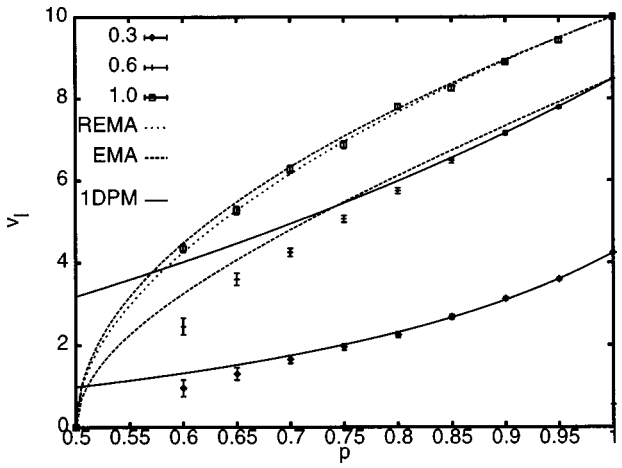

FIG. 1. Average wave-front propagation velocities of longitudinal waves in lattices with $l=1$; $m=0.005,0.01$; $w=0.3,0.6,1.0$; $E=1.0$; and the frequency 0.125. The corresponding velocities calculated from the effective-medium approximation (EMA) and the one-dimensional path model (1DPM) are shown by dotted and solid lines, respectively.

shown [16] that, in a perfect square lattice, the dispersive widening of the wave front causes a power-law decay of the form [16–19]

$$A(x)\propto x^{-1/3}. \tag{10}$$

In disordered lattices with $p\lesssim 1$, this type of decay should be observed at least for long wavelengths.

D. Numerical analysis of wave-front progation

The analytical results Eqs. (3) and (7) are compared with simulation results in Fig. 1 and a similar comparison for Eqs. (4) and (8) is shown in Fig. 2. As can be seen from Fig. 1, the effective-medium approximation (EMA) follows the simulation data well when the bond stiffness is isotropic (i.e., $w=l=1.0$). It is also evident that the model of one-dimensional path follows perfectly the simulation results for slender bonds ($w=0.3$) when $p>0.75$. For smaller p the model fails as expected. In the intermediate case ($w=0.6$) none of the models gives a very good result. Only close to $p=1$ does the model of one-dimensional paths give the correct velocity. In both Figs. 1 and 2 also the renormalized effective-medium approximation (REMA) solution is shown. As can be seen, the REMA solutions differ only a little from the EMA solutions, which indicate that the scaling regimes are small.

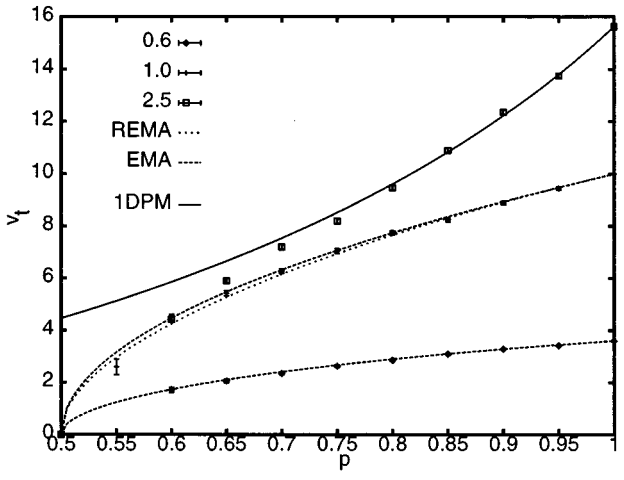

FIG. 2. Average wave-front velocities of transverse waves in lattices with $l=1$; $m=0.01,0.06$; $w=0.6,1.0,2.5$; $E=1.0$; and the frequency 0.0125. The corresponding velocities calculated from the EMA and the 1DPM are shown by dotted and solid lines, respectively.

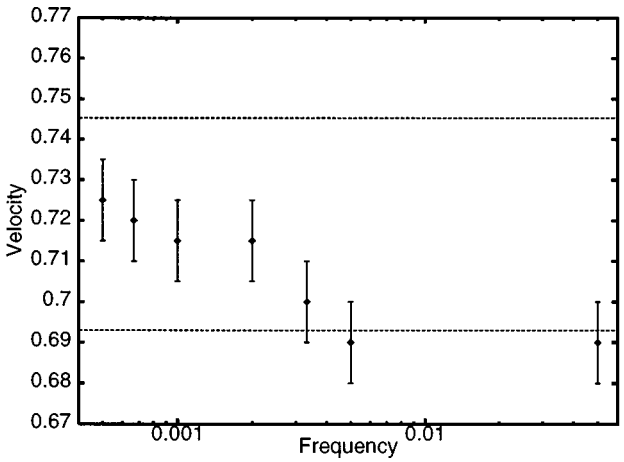

FIG. 3. Average velocity of a longitudinal wave front as a function of the driving frequency with $l=1$, $m=0.1$, $w=0.3$, $p=0.9$, and $E=1.0$. The upper and the lower lines are the prediction by the effective-medium approximation and the model of one-dimensional paths, respectively.

In Fig. 2 similar results are shown for the transverse waves. The effective-medium model works also in this case for $w\leqslant 1$. The model of one-dimensional paths gives the correct velocity for broad beams ($w=2.5$) when p is close to unity. We also expect that there should be a crossover between the two model velocities with a changing driving frequency. This crossover is, however, difficult to observe numerically. This is mainly because of the relatively small difference between the two solutions. To complete the picture, we show nevertheless in Fig. 3, how the velocity changes with frequency in the case of longitudinal waves for $w=0.3$ and $p=0.9$. This figure demonstrates a clear trend of increasing velocity at lower frequencies. Notice, however, that the effective-medium model is not very accurate for these parameter values and a 2.5% difference between the simulated velocity and the EMA prediction remains even at the lowest frequencies.

Next we test numerically the amplitude decay, i.e., Eqs. (9) and (10). In Fig. 4 we show the amplitude A as a function of x for different values of $1-p$. The parameters used are $l=1$, $m=0.0001$, $w=0.1$, and $E=1.0$. The frequency is 0.125. $A(x)$ is reasonably well approximated by an exponential decay [Eq. (9)] for small x. A crossover from the exponential to a less rapidly decaying behavior can be seen for large x and large $1-p$. This crossover phenomenon is an artifact of the dispersion relation [16]. As the effective frequency of the first displacement maximum decreases, the amount of reflection also decreases (i.e., γ increases) and

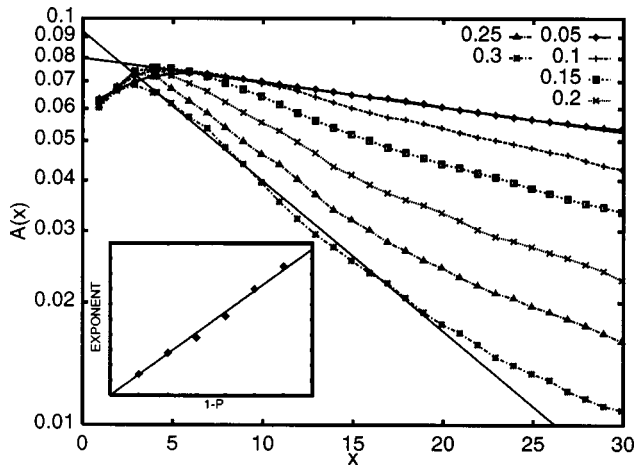

FIG. 4. Average amplitude of the wave front as a function of the distance with $l=1$; $m=0.0001$; $w=0.1,1-p=0.05,0.1,0.15,0.2,0.25,0.3$; and $E=1.0$. The frequency is 0.125. The inset shows the fitted exponents as a function of $1-p$.

eventually the frequency of the wave front becomes so small that the lattice will locally remain at equilibrium and the amplitude will decrease only according to Eq. (10). The inset in Fig. 4 proves that the exponent in Eq. (9) is indeed proportional to the dilution parameter $1-p$ for small x. The power-law decay for broader fibers ($l=1$, $m=1.0$, $w=1.0$, and $E=1.0$) is demonstrated in Fig. 5. The amplitude decay follows well Eq. (10) for large enough x.

Figures 1–5 support the velocity and amplitude decay predictions by the one-dimensional and the effective medium models in their respective regions of validity. The simulations revealed, somewhat suprisingly, also a third wave-front velocity. This velocity does not depend on the average properties of the lattice, but is instead a transient that propagates only a short distance and takes advantage of the fastest routes that exist. This is demonstrated in Fig. 6. The distances of the lattice sites from the left edge of the lattice are plotted in this figure as a function of the arrival time of the first displacement maximum at these sites. The lattice size is

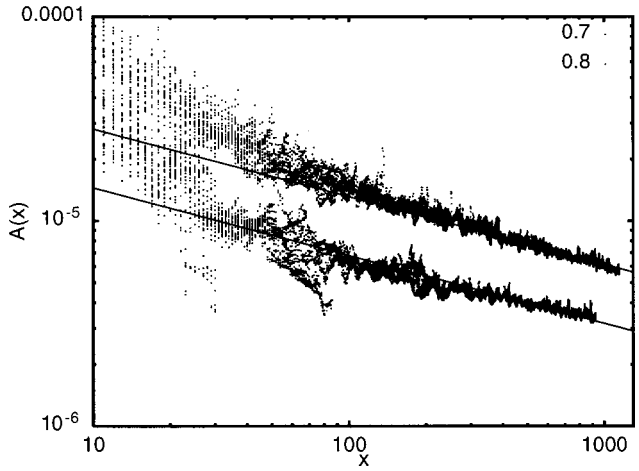

FIG. 5. Amplitude of the wave front as a function of distance with $l=1$; $m=1.0$; $w=1.0$; $p=0.7,0.8$; and $E=1.0$. The frequency is 0.125. The fitted lines are given by Eq. (10).

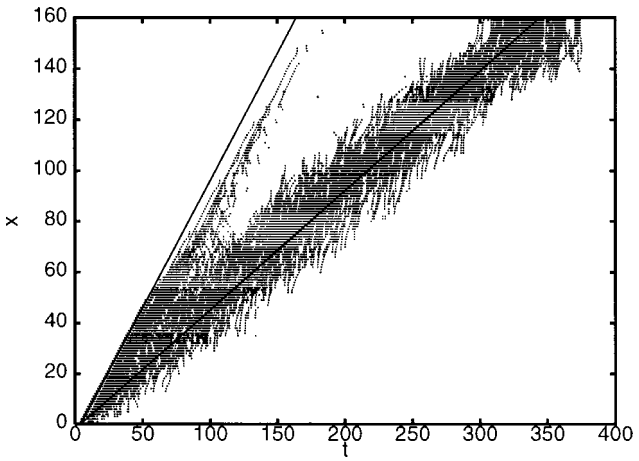

FIG. 6. Distance of the sites in a network of size 160×160 as a function of the time when the site reaches its first displacement maximum with $l=1$, $m=0.01$, $w=0.1$, $E=1.0$, $p=0.9$, and the frequency 0.0125. The lines are given by Eq. (3) with $p=0.9$ and $p=1$.

160×160 in lattice units. The network parameters are $l=1$, $m=0.01$, $w=0.1$, $p=0.9$, $E=1.0$, and frequency 0.125. Two velocity branches appear. The slower velocity is well predicted by Eq. (3) (the lower line in the figure), while the faster velocity (the upper line in the figure) is the velocity that would appear in the perfect lattice [i.e., Eq. (3) or (7) with $p=1$]. The faster signal dies out before the opposite end of the system is reached. This can also be seen in Fig. 7, where the amplitudes are plotted as a function of the distances from the left edge of the lattice for the same data as in Fig. 6. This figure shows that the amplitude of the faster signal decreases exponentially, while the amplitude of the slower signal decreases much slower for large x [i.e., according to Eq. (10)]. The fast transients are essentially signals that travel along short pieces of unbroken straight chains of beams. Their exponential decay is caused by couplings to the surroundings via the vertical bonds. The dynamics of this transient signal will be reported in more detail in Ref. [16].

IV. WAVE-FRONT ROUGHENING

So far we have only considered the mean velocity of the wave front. This does not, however, describe the dynamics

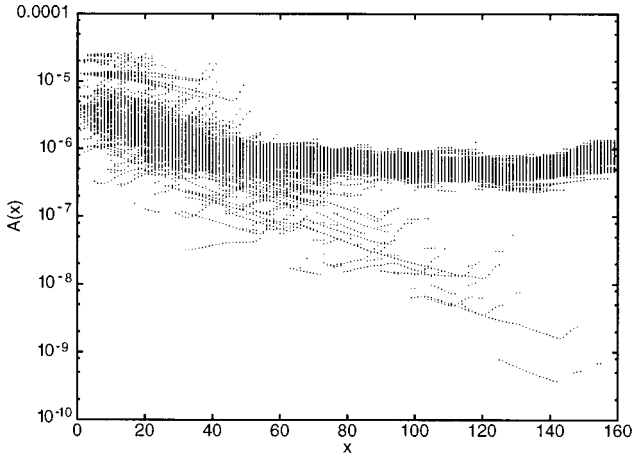

FIG. 7. Variation of the amplitude with the distance for the data of Fig. 6.

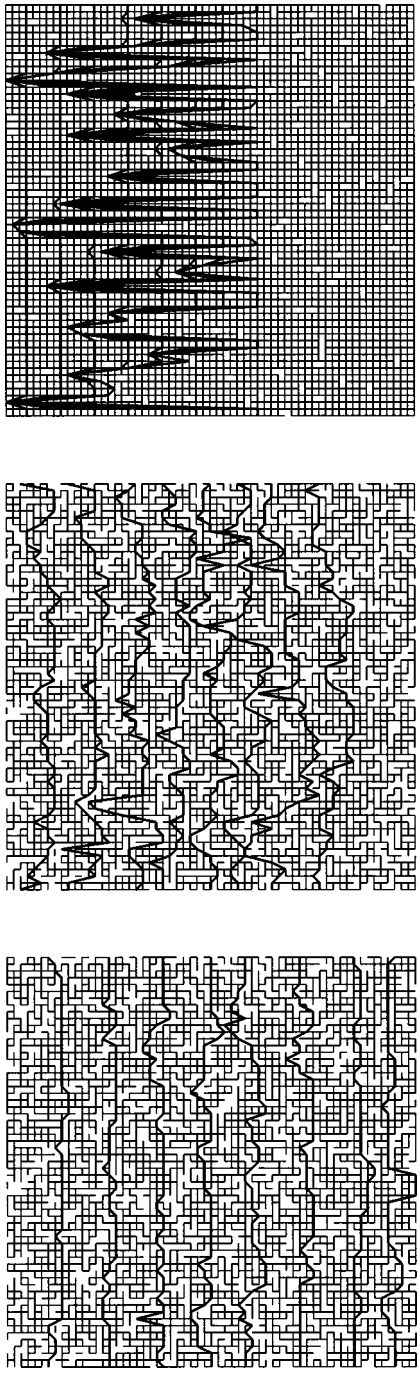

FIG. 8. Wave-front location (thick lines) at different times in lattices with (top) $w=0.001$ and $p=0.98$, (middle) $w=1.0$, and $p=0.7$, and (bottom) $w=20.0$ and $p=0.7$.

of the front completely. Caused by the disorder, the initially straight front will get rough as it propagates. This is demonstrated for three examples in Fig. 8. The wave fronts propagate from left to right; as time evolves the initially flat fronts become more and more complicated. Notice the difference in roughness between the last two cases, arising from a much higher bending stiffness in the latter.

It would be reasonable to expect that the roughening of the wave front would belong to one of the usual universality classes. Simulations show, however, that this is not the case. Instead, if one considers in a similar fashion the early time and the asymptotic interface widths, a very complicated behavior is encountered. We believe that this is due to the fact that the wave-front velocity behaves differently in the two limits, as explained above. The situation is further complicated by the appearance of the transient velocity (cf. Fig. 6).

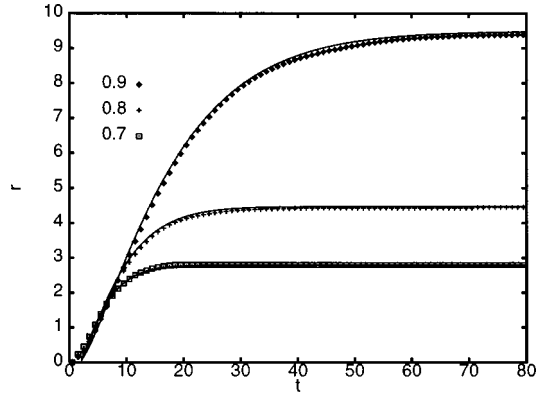

FIG. 9. Roughness in lattices with $l=1$; $m=10^{-6}$; $w=0.001$; $E=1.0$; $p=0.7,0.8,0.9$, and the frequency 0.125. The lines are given by Eq. (12).

In the limit of a vanishing axial or bending stiffness, it is possible to calculate the dynamics of the roughening exactly. In the case of longitudinal waves and vanishing bending stiffness, the wave will travel poorly in the y direction along the vertical bonds and the wave front can be considered to travel along independent straight paths until a missing bond is encountered and the propagation stops. This means that the average velocity will decrease exponentially with time (t). The average location of the wave front $x_m(t)$ is then given by

$$x_m(t)=\frac{p(1-p^{vt})}{1-p}, \tag{11}$$

where v is the wave velocity in the case when $p=1$ [given by Eqs. (3) and (7)]. When $t\to\infty$, x_m will approach the value $p/(1-p)$. The roughness $r(t)$ of the wave front is given by

$$\begin{aligned} r^2(t)(1-p)^2=&p^2[1-p^{vt}]^2[1-p^{vt+1}]+[p-p^2+2p^{vt}] \\ &\times[1-(vt+1)p^{vt}+vtp^{vt+1}]+p^2(1-p) \\ &\times vt(vt+1)[p^{vt}-p^{vt-1}]. \end{aligned} \tag{12}$$

When $t\to\infty$ the roughness $r(t)$ approaches the value $\sqrt{p}/(1-p)$, which holds for all p except for $p=1$. A comparison of Eq. (12) with numerical results is shown in Fig. 9. In this figure $l=1$, $m=10^{-6}$, $w=0.001$, $E=1.0$, and the frequency is 0.125. It is evident that Eq. (12) fits the simulation results very well. Two further observations can also be made based on the Fig. 9: There is, in terms of the usual interface growth models, a trivial pinning transition that takes place in the infinite time limit and the interface width does not depend on the system size. Interface dynamics is thus similar to that of the random deposition model, in which local fluctuations set the time dependence.

With a nonzero bending stiffness the situation becomes immediately more complicated. At early enough times the front behavior may in some cases be of the Edwards-Wilkison type ($\beta\sim 1/4$), i.e., there is a parallel correlation length along the interface dictated by diffusive dynamics. At

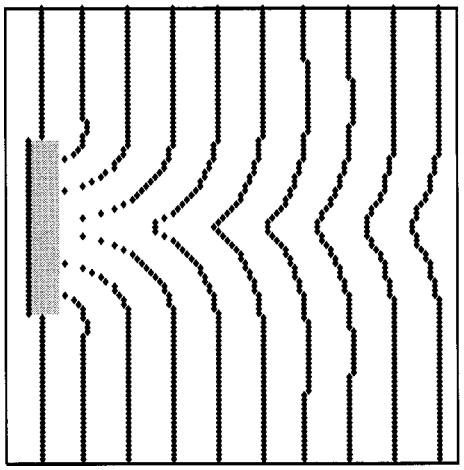

FIG. 10. Wave front at ten different times in a network with bonds only diluted in the shaded square close to the left boundary, $l=1$, $m=0.01$, and $w=1.0$.

longer time scales, however, there is no typical saturation behavior manifested by a size-dependent interface width.

We next consider the case when the bending and axial stiffnesses are equal. In this case we are not able to calculate the roughness exactly. We expect, however, that the lattice will behave more or less like a continuous medium with randomly located holes. Then the wave-front roughness should be governed by the Huygens principle. This is demonstrated in Fig. 10. The wave-front patterns in this figure are not exactly spherical shapes as predicted by the Huygens principle, but a slight distortion of the shape is expected because the effective stiffness of the network is lower than the average close to a hole. Furthermore, the velocity is not quite isotropic, which also causes a distortion of the normal spherical shape.

The roughness of an interface governed by the Huygens principle has been analyzed earlier as a model of sputter deposition for amorphous films [20]. A rough interface will be subject to a smoothing effect caused by the lateral, synchronous growth of peaks on the interface. This will cause height differences δh, a distance x_0 apart, to be smoothened out in a time t such that

$$\delta h \propto x_0^2/vt, \tag{13}$$

where v is the interface propagation velocity. Roughening of the interface will be induced by the uncorrelated random vacancies in the lattice. The average height fluctuations, resulting from this uncorrelated noise, will increase like

$$\delta h \propto (vt)^{1/2}. \tag{14}$$

The roughness of an initially flat interface, induced by missing bonds, will therefore increase like $r \propto t^{1/2}$. Roughness will then, however, reach a state when there is a balance between the two opposite mechanisms described by Eqs. (13) and (14). This happens when

$$\delta h \propto x_0^2/(\delta h)^2 \Rightarrow \delta h \propto x_0^{2/3}. \tag{15}$$

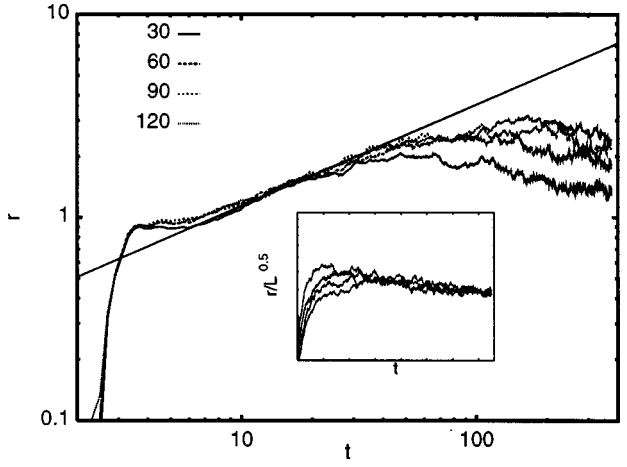

FIG. 11. Averaged wave-front roughness as a function of time in lattices with $p=0.7$ and vertical heights $L_y=30,60,90,120$; $l=1$, $m=1.0$, $w=1.0$, $E=1.0$, and the frequency is 0.125. The fitted line is given by $r(t) \propto t^{1/2}$. The inset shows the same data on a semilogarithmic scale, with the y axis rescaled by $L^{-0.5}$.

In a lattice of linear size L the maximum height difference is therefore proportional to $L^{2/3}$, which means that the roughness exponent is 2/3. The corresponding crossover time scale is

$$t_{\text{crossover}} \propto x_0^{4/3}/v. \tag{16}$$

What was not taken into account above, however, is the effective decrease in the frequency of the first displacement maximum. For lower frequencies, the details of the lattice are not as easily ''felt'' by the wave front. Intuitively, we would expect this effect to have a decreasing effect on the roughness. In Fig. 11 we show the roughness obtained by simulations for networks of sizes 30×300, 60×300, 90×300, and 120×300, with $m=w=E=1.0$, $p=0.7$, and the frequency 0.125. The first wave front leaves the left edge of the network at $t=2$. As can be seen from the figure, the transient signal affects the roughness of the front for $t<10$. For $10<t<50$ the roughness grows diffusively according to $t^{1/2}$, as predicted by Eq. (14). For late times the roughness *decreases*, which demonstrates that the decreasing frequency

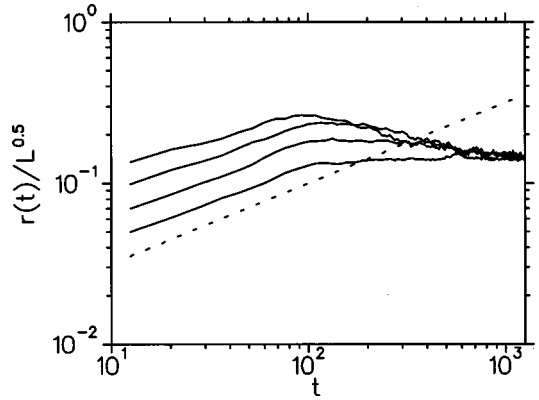

FIG. 12. Averaged wave-front roughness as a function of time in TLM lattices with $p=0.85$ and vertical heights $L_y=30,60,120,240$; the driving frequency is 0.314. The dashed line is given by $r(t) \propto t^{1/2}$.

of the wave front has a strong effect on roughness. The roughness exponent 2/3 fits the data for the two largest systems of Fig. 11, but the two smaller systems (30×300, and 60×300) have an asymptotic roughness that is too high to follow Eq. (15). We expect that these two small systems are not yet in the scaling region. The roughness exponent that fits best all the simulation data is therefore smaller than 2/3 (i.e., around 0.5), which is demonstrated by the inset in Fig. 11.

To further test Eqs. (14) and (15) we also used a numerical algorithm [transmission line method (TLM) wave automaton], that solves the classical wave equation by directly applying Huygens's principle [21]. Using this model, we again found that roughness grows diffusively ($t^{1/2}$), but the roughness exponent is lower than the 2/3 predicted by Eq. (15). A best fit to the data gave a roughness exponent around 0.5 (Fig. 12).

V. DISCUSSION AND CONCLUSIONS

In summary, we have demonstrated that the propagation velocity and the amplitude decay of the first displacement maximum in randomly diluted square lattices of elastic beams can be largely understood within two simple models. In the limit of vanishing axial or bending modulus, a one-dimensional model correctly describes the dynamics of the wave front. When the bending and the axial moduli are roughly equal, an effective-medium approximation combined with continuum elasticity theory is sufficient for describing the wave-front propagation.

The roughness of the wave front can be exactly calculated in the limit of a vanishing axial or bending modulus. In this limit the first wave front is always localized and the average wave-front width is finite. As the time evolution is governed by Poissonian fluctuations, this is a random-deposition–equivalent phenomenon for wave fronts. For beams that have a nonvanishing bending stiffness, the two-dimensional character of wave propagation makes the roughening process resemble ''standard'' kinetic roughening phenomena. However, the dynamic behavior cannot be mapped to the standard models, except perhaps at early times.

For roughly equal bending and axial moduli, the wave-front roughness grows initially like $t^{1/2}$. For late times, Huygens's principle suggests a roughness exponent 2/3, but simulations gave an exponent close to 0.5. This discrepancy is still not fully understood but is probably due to finite-size effects.

[1] L. D. Landau and E. M. Lifshitz, *Theory of Elasticity* (Pergamon, Oxford, 1958).

[2] A. L. Fetter and J. D. Walecka, *Theoretical Mechanics of Particles and Continua* (McGraw-Hill, New York, 1980).

[3] *Scattering and Localization of Classical Waves in Random Media*, edited by P. Sheng (World Scientific, Singapore, 1990).

[4] A.-L. Barabasi and H. E. Stanley, *Fractal Concepts in Surface Growth* (Cambridge University Press, Cambridge, 1995)

[5] J. Krug and H. Spohn, in *Solids Far From Equilibrium*, edited by C. Godereche (Cambridge University Press, Cambridge, 1991).

[6] F. Family, Physica A **19**, L441 (1993).

[7] S. F. Edwards and D. R. Wilkinson, Proc. R. Soc. London, Ser. A **381**, 17 (1982).

[8] M. Kardar, G. Parisi, and Y.-C Zhang, Phys. Rev. Lett. **56**, 889 (1986).

[9] S. Feng, L. Golubovic, and Y.-Z. Zhang, Phys. Rev. Lett. **65**, 1028 (1990).

[10] W. Nowacki, *Theory of Micropolar Elasticity* (Springer-Verlag, Udine, 1972).

[11] H. J. Herrmann and S. Roux, in *Statistical Models for the Fracture and Elasticity of Disordered Media*, edited by H. J. Herrmann and S. Roux (North-Holland, Amsterdam, 1990).

[12] This is the same formalism as that used in the dynamic finite element method.

[13] S. Kirkpatrick, Rev. Mod. Phys. **45**, 574 (1973).

[14] M. Born and K. Huang, *Dynamical Theory of Crystal Lattices* (Oxford University Press, New York, 1954).

[15] M. Sahimi, *Applications of Percolation Theory* (Taylor & Francis, London, 1994).

[16] M. Kellomäki, J. Åström, and J. Timonen (unpublished).

[17] L. Brillouin, *Wave Propagation and Group Velocity* (Academic, New York, 1960).

[18] I. Tolstoy, *Wave Propagation* (McGraw-Hill, New York, 1973).

[19] A. Segel and G.H. Handelman, *Mathematics Applied to Continuum Mechanics* (Macmillan, New York, 1977).

[20] C. Tang, S. Alexander, and R. Bruinsma, Phys. Rev. Lett. **64**, 772 (1990).

[21] P. O. Luthi, B. Chopard, and J.-F. Wagen, *Lecture Notes in Computer Science* (Springer, Berlin, 1996).